Dalton Transactions

Cite this: *Dalton Trans.*, 2011, **40**, 6555

www.rsc.org/dalton

PAPER

Chemistry of 11-vertex rhodathiaboranes: reactions with monodentate phosphines†

Beatriz Calvo,[a] Martin Kess,[a,c] Ramón Macías,*[a] Carmen Cunchillos,[b] Fernando J. Lahoz,[a,b] John D. Kennedy[d] and Luis A. Oro[a,b,e]

Received 2nd March 2011, Accepted 12th April 2011
DOI: 10.1039/c1dt10355e

The reaction of [8,8-$(PPh_3)_2$-*nido*-8,7-$RhSB_9H_{10}$] (**1**) with PR_3 in a 1 : 2 ratio affords mixtures that contain the mono-substituted *bis*-PR_3-ligated rhodathiaboranes [8,8-(PPh_3)(L)-*nido*-8,7-$RhSB_9H_{10}$] [L = PMe_2Ph (**5**), PMe_3 (**6**)] and the corresponding *tris*-PR_3-ligated compounds [8,8,8-$(L)_3$-*nido*-8,7-$RhSB_9H_{10}$] [L = PMe_2Ph (**7**), PMe_3 (**8**)]. These latter species are more conveniently prepared from the reaction of **1** with three equivalents of the monodentate phosphines, PMe_2Ph and PMe_3. Reaction between **1** and $PMePh_2$ in a 1 : 2 ratio yields the disubstituted rhodathiaborane [8,8-$(PMePh_2)_2$-*nido*-8,7-$RhSB_9H_{10}$] (**4**), whereas the use of three equivalents of phosphine leads to the formation of B-ligated eleven-vertex [8,8,8-$(PMePh_2)_2$(H)-*nido*-8,7-$RhSB_9H_9$-9-$(PMePh_2)$] (**9**). Compounds **4–9** have been characterized by NMR spectroscopy, and the structures of **8** and **9** confirmed by X-ray diffraction analyses. The characterization of the cluster compounds has been aided by the use of DFT calculations on some of the species. Variable-temperature NMR studies have demonstrated a lability of the $PMePh_2$ ligands in compounds **4** and **9**, providing mechanistic insights about the ligand substitutional chemistry in these eleven-vertex rhodathiaboranes.

Introduction

Recent research has led to the discovery that the eleven-vertex rhodathiaborane [8,8-$(PPh_3)_2$-*nido*-8,7-$RhSB_9H_{10}$] (**1**)[1] reacts with pyridine to form the B-pyridine-substituted hydridorhodathiaborane [8,8,8-$(PPh_3)_2$(H)-*nido*-8,7-$RhSB_9H_9$-9-(NC_5H_5)] (**2**), which undergoes thermal dehydrogenation to afford [1,1-$(PPh_3)_2$-*closo*-1,2-$RhSB_9H_8$-3-(NC_5H_5)] (**3**).[2] Compounds **2** and **3** have been shown to be active catalyst precursors for the homogeneous hydrogenation and isomerization of alkenes.[3] In addition, reactivity studies of the reaction of alkynes with **2** have demonstrated that its dehydrogenation can promote the oxidative addition of *sp* C–H bonds,[4] suggesting that other E–H bonds, in for example alkanes, silanes, or boranes, could also be activated by modifying the reaction conditions and/or by an appropriate tailoring of the clusters.

The ease of preparation, the versatility, and the stability of these eleven-vertex cluster compounds make them attractive candidates for homogeneous catalyst precursors.[3,4] This consideration prompted us to examine how we might modify the *exo*-polyhedral phosphine-ligand sphere in order to explore the reactivity of new phosphine-ligated derivatives of **2**, the overall target being the optimization of the catalytic activity of these polyhedral compounds. In this regard, it has previously been demonstrated that the rhodathiaborane **1** undergoes facile substitution of PPh_3 by other monodentate, and also bidentate, phosphines;[5,6] herein we deal with reactions of **1** with the monodentate phosphines $PMePh_2$, PMe_2Ph and PMe_3.

Results and discussion

Reactions of [8,8-$(PPh_3)_2$-*nido*-8,7-$RhSB_9H_{10}$] (1) with $PMePh_2$, PMe_2Ph and PMe_3

Treatment of the *bis*-(PPh_3) compound **1** with two equivalents of $PMePh_2$ affords the disubstituted rhodathiaborane, [8,8-$(PMePh_2)_2$-*nido*-8,7-$RhSB_9H_{10}$] (**4**). In contrast, the use of two equivalents of PMe_2Ph or PMe_3 gives mixtures that contain both the monosubstituted *bis*-(phosphine) species, [8,8-(PPh_3)(L)-*nido*-8,7-$RhSB_9H_{10}$], where L = PMe_2Ph (**5**) or PMe_3 (**6**), together with the products of addition of a third phosphine at the metal, *viz.*

[a]*Instituto Universitario de Catálisis Homogénea, Universidad de Zaragoza, Zaragoza, Spain. E-mail: rmacias@unizar.es; Fax: +34 976 762 453; Tel: +34 976 761 146*
[b]*Departamento de Química Inorgánica, Instituto de Ciencia de Materiales de Aragón, Universidad de Zaragoza-Consejo Superior de Investigaciones Científicas, Zaragoza, Spain*
[c]*Institute of Inorganic Chemistry, Lehrstuhl II, Am Hubland, 97074, Würzburg*
[d]*School of Chemistry, University of Leeds, Leeds, UK, LS2 9JT*
[e]*King Fahd University of Petroleum and Minerals, KFUPM Visiting Professor, Dhahran 31261, Saudi Arabia*

† Electronic supplementary information (ESI) available: Experimental and DFT-calculated NMR data for **1**, **6** and **8**; NMR spectra of the reaction of **1** with PPh_2Me at different temperature, as well as **9** with PPh_3; DFT-calculated coordinates for **1**, **6**, **8** and **9**. CCDC reference numbers 814662–814663. For ESI and crystallographic data in CIF or other electronic format see DOI: 10.1039/c1dt10355e

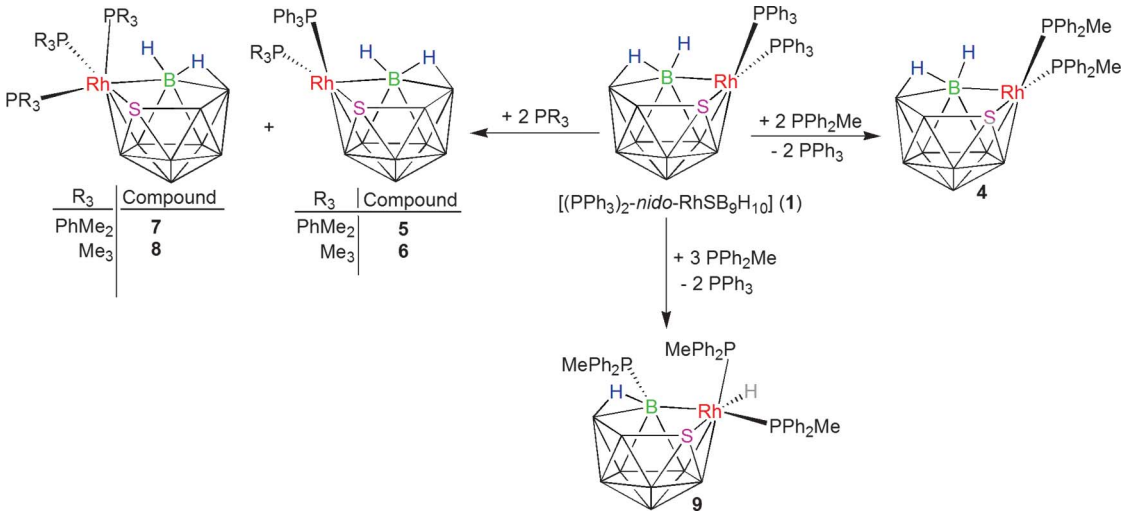

Scheme 1

the *tris*-(phosphine) species [8,8,8-(L)$_3$-*nido*-8,7-RhSB$_9$H$_{10}$], where L = PMe$_2$Ph (**7**) or PMe$_3$ (**8**). These last two *tris*-(phosphine) {Rh(PR$_3$)$_3$}-containing compounds are more conveniently prepared from the reactions of **1** with three equivalents of phosphine. In an interesting contrast, the same reaction, but now with PMePh$_2$ in a 1 : 3 rhodathiaborane : phosphine molar ratio, yields the boron-substituted hydridorhodathiaborane [8,8,8-(PMePh$_2$)$_2$(H)-*nido*-8,7-RhSB$_9$H$_9$-9-(PMePh$_2$)] (**9**). Scheme 1 illustrates these results, and it can be used as a guide throughout the paper.

The 160 MHz ^{11}B–{^{1}H} NMR spectra of the PMe$_3$ and PMe$_2$Ph mixed *bis*-(phosphine) species **5** and **6** (see Table 1) show eight peaks in a 1 : 1 : 2 : 1 : 1 : 1 : 1 : 1 intensity ratio, slightly shielded [mean δ(^{11}B) *ca.* −6 ppm] with respect to compound **1** [mean δ(^{11}B) *ca.* −4 ppm.]. The signal of relative intensity 2 results from the accidental coincidence of resonances from two chemically different boron sites: these are effectively distinguished individually by ^{1}H–{^{11}B(selective)} experiments. In contrast, the expected nine signals are all resolved in the ^{11}B spectra of the *bis*-(PMePh$_2$) species **4** and they exhibit the largest overall shielding in the series [mean δ(^{11}B) *ca.* −10 ppm], which may reflect a different electron contribution of the two PPh$_2$Me ligands in **4** compared to the mixed pairs of phosphines, {(PPh$_3$)(PMe$_3$)} and {(PPh$_3$)(PMe$_2$Ph)} in the monosubstituted counterparts **5** and **6**. The ^{1}H–{^{11}B} spectra of these new PR$_3$-ligated rhodathiaboranes show that there is also a shielding of the BHB bridging-hydrogen atom with respect to the PPh$_3$ derivative **1**, with the higher shielding [at δ(^{1}H) −0.46 ppm] being that of compound **4**. It has been suggested that higher-field shifts of the BHB proton resonances in *nido* eleven-vertex rhodathiaboranes of this type correlate with a negative charge build-up on the metal centers.[7] Thus, the trend of high-field shifts found in the series of rhodathiaboranes, **1**, **4**, **5** and **6** could be related, at least in part, to an increase in the electron density at the rhodium centre: {Rh(PPh$_3$)$_2$} < {Rh(PPh$_3$)(PMe$_2$Ph)} < {Rh(PPh$_3$)(PMe$_3$)} < {Rh(PMePh$_2$)$_2$}.

Table 1 ^{11}B and ^{1}H–{^{11}B} NMR data for the *bis*-phosphine compounds **5** and **6** in CDCl$_3$ at room temperature

	5		**6**	
Assignment[a]	δ(^{11}B)	δ(^{1}H)	δ(^{11}B)	δ(^{1}H)
3	+15.5	+3.65	+15.8	+3.74
9	+10.6	+3.20	+10.3	+3.10
11	+2.6[b]	+3.24	+2.2[b]	+3.22
6		+2.37		+2.29
4	−1.3	+3.09	−1.3	+3.02
5	−8.5	+2.29	−8.2	+2.39
1	−18.5[c]	+0.83	−23.2	+1.55
10	−24.4	+1.14	−25.6	+0.91
2	−28.2[d]	+0.83	−27.7	+0.70
μ-(9,10)		−1.30		−1.33

[a] Assignments based on ^{1}H–{^{11}B} selective experiments and comparison with **1**. [b] Accidentally coincident ^{11}B resonances for B(6) and B(11). [c] ^1J(^{11}B–^{1}H) *ca.* 150 Hz. [d] ^1J(^{11}B–^{1}H) *ca.* 141 Hz.

The ^{31}P-{^{1}H} spectra of the PMe$_3$ and PMe$_2$Ph mixed-ligand PPh$_3$ compounds **5** and **6** at room temperature exhibit two doublets of doublets, which conform to the asymmetric structure of these cluster compounds. The signals around δ(^{31}P) *ca.* +25 ppm correspond to the PPh$_3$ ligands, whereas the resonances of the methyl-ligated phosphines are at higher field. In contrast, the *bis*-(PMePh$_2$)-ligated rhodathiaborane **4** exhibits a very broad signal in the ^{31}P-{^{1}H} spectrum at room temperature: this signal splits into two doublets of doublets at lower temperatures, resembling the pattern of **5** and **6**. The ^{1}H NMR spectrum of **4** also shows a temperature-dependent behaviour that at high temperatures renders equivalent the two methyl resonances of the PMePh$_2$ ligands, and leads to the coalescence in pairs of some of the BH terminal hydrogen resonances. Therefore, the NMR data for **4** at different temperatures are suggestive of an intramolecular dynamic process, which resembles the fluxional behavior of other analogous *nido*-structured eleven-vertex metallaheteroboranes {MEB$_9$} where M = Pt or Rh and E = S, N or C (see Table 2). The activation energies for these processes are readily estimated from the temperatures at which peak-coalescences are observed in the NMR spectra. This type of non-rigid behaviour has become increasingly recognised in eleven-vertex metallaheteroboranes that incorporate formally unsaturated pseudo-square-planar Rh(I) or Pt(II) vertices; and recent DFT calculations have revealed that *isonido*- and *closo*-shaped clusters are points along the reaction coordinate of this inter-enantiomeric fluxional process.[8]

Table 2 Activation energies for the fluxional process of eleven-vertex *nido*-metallaheteroboranes

Compound	$\Delta G^{\ddagger}$ (kJ mol^{-1})	Reference
$[(PPh_3)_2RhSB_9H_{10}]$ (**1**)	58	1
$[(PMePh_2)_2RhSB_9H_{10}]$ (**4**)	52	This work
$[(dppp)RhSB_9H_{10}]$	53	5
$[(dppp)RhSB_9H_9(OEt)]^a$	>64	5
$[(PPh_3)_2RhNB_9H_{11}]$	46	8
$[(PMe_2Ph)_2PtCB_9H_{11}]$	62	8
$[(PMe_2Ph)_2PtCB_9H_{10}(OEt)]$	>75	9

^{a} dppp = $Ph_2P(CH_2)_3PPh_2$

The *tris*-(PMe_2Ph)-ligated *nido*-rhodathiaborane **7** has been reported previous to this work,[10] but for convenience of comparison, its spectroscopic data are described here together with those of **8**. The molecular structure of **7** was also determined by single-crystal X-ray diffraction in the previous work.[10] We now report the crystallographic analysis of the new *tris*-(PMe_3)-ligated analogue **8** (*vide infra*). The ^{11}B and ^{1}H NMR data for both compounds are listed in Table 3. The proton spectra of each cluster exhibits nine signals in the positive region that can be assigned to the nine BH units of the cluster, and a singlet at the highest-field that corresponds to the BHB hydrogen atom. Due to the overlapping of some resonances, the ^{11}B spectra do not show the separated nine-peak pattern expected for the asymmetric structure of these clusters; however, selective ^{1}H–{^{11}B} decoupling experiments enabled the indirect resolution of the individual components of the broad signals of relative intensity 2 and 3 in the spectra of **7** and **8**, respectively (Table 3).

Although **7** and **8** each bear a third phosphine ligand on the metal centre, there is no overall significant shift towards higher fields [mean $\delta(^{11}B)$ –6 ppm] with respect to the monosubstituted *bis*-(phosphine) parent compounds **5** and **6**, suggesting that the additional electron density donated by the third ligand is highly localized at the rhodium centre, and that the electronic structures within the clusters of **5**, **6**, **7** and **8** are all very similar. In this regard, and according to the rationale described above, the shift to higher field of more than 2.6 ppm in the ^{1}H NMR resonance of the BHB hydrogen atoms in **7** and **8** may reflect an increase in the electron density at the rhodium centre; differential neighbouring-group magnetic anisotropic effects arising from P-phenyl *versus* P-methyl substituents on the phosphines may also play a role. In any event,

Table 3 ^{11}B and ^{1}H NMR data for the *tris*-phosphine compounds **7** and **8** in $CDCl_3$ at room temperature. In brackets are the DFT/GIAO-calculated ^{11}B nuclear shielding values for **8**

	7		**8**	
Assignment	$\delta(^{11}B)$	$\delta(^1H)$	$\delta(^{11}B)$ [DFT]	$\delta(^1H)$
6	+13.5	+4.03	+13.0 [+13.8]	+3.95
9	+7.1	+3.79	+6.1 [+12.2]	+3.29
3	+7.1	+2.14	+6.1 [+11.9]	+3.12
4	+5.3	+3.55	+6.1 [+8.1]	+1.93
11	–1.1	+2.40	–2.3 [+1.8]	+2.83
10	–14.1	+2.40	–15.4 [–14.0]	+1.84
5	–15.5	+1.97	–15.5 [–15.7]	+1.70
1	–21.2	+1.93	–22.9 [–20.9]	+1.70
2	–27.0	+1.24	–27.1 [–28.6]	+1.20
μ-(9,10)		–3.98		–3.75

this large high-field shift in the BHB bridging proton resonance is diagnostic of formation of {RhL_3} *tris*-ligated eleven-vertex rhodathiaboranes *versus* their {RhL_2} *bis*-ligated counterparts. For **7** and **8**, the presence of three phosphine ligands bound to the rhodium atom is clear in the ^{31}P-{^{1}H} NMR spectra that show three signals in a 1 : 1 : 1 relative intensity ratio. For compound **8**, the comparison of the spectrum at 223 K with that at 300 K is a nice illustration of the "thermal decoupling" of the boron nuclei,[11] which leads to a resolution of the coupling constants $^2J(^{31}P–^{31}P)$ at low temperature that do not manifest at room temperature (see Fig. S3 in the supporting information†).

The characterization of the new B-ligated hydridorhodathiaborane **9** has also been carried out by X-ray diffraction analysis (*vide infra*) and by NMR spectroscopy. The ^{11}B–{^{1}H} NMR spectrum shows eight peaks in a 2 : 1 : 1 : 1 : 1 : 1 : 1 : 1 intensity ratio, with the peak of relative intensity 2 resulting from an accidental overlap of two resonances (Table 4). These latter two are effectively distinguished by ^{1}H–{^{11}B} selective decoupling experiments as mentioned above. Diagnostic of the formation of the eleven-vertex hydrido-*nido*-rhodathiaborane are the ^{1}H–{^{11}B} NMR signals at $\delta(^1H)$ –1.79 and –12.10 ppm, which correspond to the BHB bridging hydrogen atom and the Rh-H hydride ligand, respectively. In the ^{31}P-{^{1}H} NMR spectrum, compound **9** exhibits three resonances with the highest-field signal being significantly broader than the other two, and, therefore, assigned to the $PMePh_2$ ligand directly bound to the boron vertex B(9).

Molecular structures of $[(PMe_3)_3RhSB_9H_{10}]$ 8 and $[(PMePh_2)_2(H)RhSB_9H_9(PMePh_2)]$ 9

The crystal and molecular structures of **8** and **9** were established by single-crystal X-ray crystallography. A summary of selected derived interatomic distances and angles for these two rhodathiaboranes are in Table 5, and drawings of these molecules are in Fig. 1 and 2. The molecular structure of each compound is based on an eleven-vertex *nido*-arrangement that has a pentagonal face, formally obtained by the removal of one vertex from an icosahedron. Both **8** and **9** are formally (11 + 2) skeletal-electron-pair (sep) *nido*-rhodathiaborane analogues of the hypothetical parent borane $B_{11}H_{15}$: three bridging hydrogen atoms and three BH

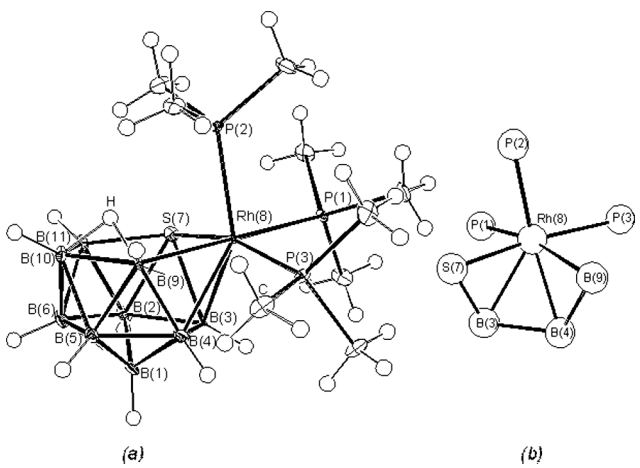

Fig. 1 (a) ORTEP-type drawing of compound **8** (50% thermal ellipsoids for non-hydrogen atoms); (b) detail of the {$Rh(PMe_3)_3$}-to-{SB_9H_{10}} metal-to-cluster coordination sphere.

Table 4 ^{11}B, ^{1}H and ^{31}P NMR data for compound **9** in $CDCl_3$ at room temperature compared with the corresponding DFT-calculated chemical shifts

Cluster data

Assignment[a]	$\delta(^{11}B)$ (ppm)		$\delta(^{1}H)$ (ppm)	$^{1}J(^{11}B–^{1}H)$ (Hz)
	Measured	Calculated		
3, 6	+4.2	+8.3, +7. 7	+2.81, +3.58	122
4	–0.8	+2.7	+3.01	127
11	–2.8	+0.5	+3.11	
9	–4.0	–0.9	[B-PPh_2Me]	
5	–7.5	–11.3	+1.86	122
2, 10	–21.2	–22.3, –22.8	+1.31	
1	–25.1	–24.5	+1.58	132
μ (9, 10)			–1.79	
8			–12.10 [Rh-H]	

PPh_2Me data in $CDCl_3$ solution[b]

Assignment[c]	$\delta(^{31}P)$ (ppm)		$^{1}J(^{103}Rh–^{31}P)$ (Hz)	$\delta(^{1}H)$ (ppm)	$^{2}J(^{31}P–^{1}H)$ (Hz)
	Measured[d]	Calculated			
P(1)	+15.3	+14.7	85	+1.72	7.4
P(2)	+9.6	+10.6	128	+1.64	6.8
P(3)	–2.9[e]	–7.5	—	+1.67	11.2

[a] Based on $^{1}H–\{^{11}B(sel)\}$experiments and DFT calculations [b] Measured at 273 K. [c] Based on $^{1}H–\{^{31}P(selective)\}$ experiments and DFT-calculations. [d] Broad signals: $^{2}J(^{31}P–^{31}P)$ coupling constants not observed $^{1}J(^{31}P–^{11}B) = 129$ Hz [e] Broad *pseudo*-doublet, $^{1}J(^{31}P–^{11}B) = 129$ Hz

Table 5 Selected distances (Å) and angles (°) for **8** and **9** with standard uncertainties (s.u) in parentheses

	8	**9**
Rh(8)–S(7)	2.3736(7)	2.4172(5)
Rh(8)–P(1)	2.4016(4)	2.3206(6)
Rh(8)–P(2)	2.3619(4)	2.3175(5)
Rh(8)–P(3)	2.2869(4)	n/a
Rh(8)–B(3)	2.291(3)	2.238(2)
Rh(8)–B(4)	2.2517(18)	2.224(2)
Rh(8)–B(9)	2.2339(17)	2.218(2)
S(7)–B(2)	2.0012(19)	1.970(3)
S(7)–B(3)	2.047(3)	2.062(2)
S(7)–B(11)	1.9140(19)	1.930(3)
P(3)–B(9)	n/a	1.943(2)
B(6)–B(11) (shortest)	1.739(3)	1.742(4)
B(2)–B(3) (longest)	1.885(4)	1.907(4)
B–B (average)	1.795(1)	1.796(1)
P(1)–Rh(8)–P(2)	96.256(14)	100.810(19)
P(1)–Rh(8)–P(3)	93.443(15)	n/a
P(1)–Rh(8)–B(9)	174.29(5)	159.43(6)
P(1)–Rh(8)–H(1)	n/a	80.3(12)
P(2)–Rh(8)–P(3)	97.946(15)	n/a
P(2)–Rh(8)–B(3)	148.61(8)	147.57(6)
P(2)–Rh(8)–B(4)	133.44(5)	144.25(6)
P(2)–Rh(8)–H(1)	n/a	89.1(12)
S(7)–Rh(8)–P(1)	86.400(15)	99.077(19)
S(7)–Rh(8)–P(2)	98.40(2)	95.149(18)
S(7)–Rh(8)–P(3)	163.57(2)	n/a
S(7)–Rh(8)–B(9)	88.04(4)	88.79(5)
Rh(8)–B(9)–P(3)	n/a	124.17(11)

groups on the pentagonal open face of $B_{11}H_{15}$ are formally replaced by a sulfur atom, a $\{B(PMePh_2)\}$ vertex and the $\{RhH(PMePh_2)_2\}$ fragment to give **9**; two BH groups and three of the four bridging hydrogen atoms of $B_{11}H_{15}$ are formally replaced by a sulfur atom and the $\{Rh(PPh_2Me)_3\}$ fragment in **8**.

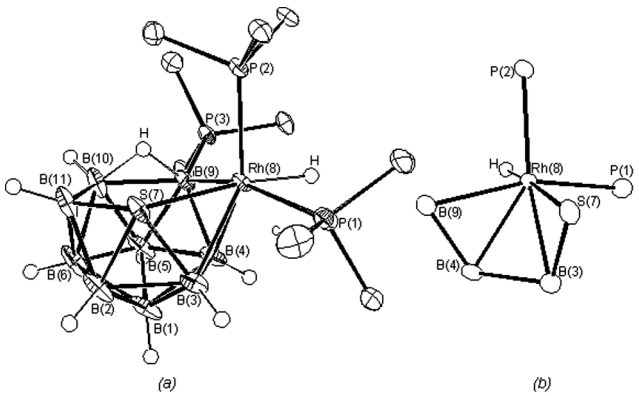

Fig. 2 (a) ORTEP-type drawing of compound **9** (50% thermal ellipsoids for non-hydrogen atoms); (b) detail of the $\{Rh(PMePh_2)_2H\}$-to-$\{SB_9H_9(PMePh_2)\}$ metal-to-cluster coordination sphere.

The interboron distances are all within normal ranges for polyhedral boron-containing clusters, although the larger distances in excess of 1.9 Å for the B(2)–B(3) vectors that flank the sulfur atoms should perhaps be noted. The Rh–P distances across the whole series of eleven-vertex rhodathiaboranes **1**, **2**, **7**, **8** and **9** vary from the shortest in compound **8** at 2.2868(5) Å to the longest in **7** at 2.4539(8) Å.[10] In each of these compounds, the longest Rh–P linkage is with the phosphine ligand that is *trans* to a boron vertex: B(9) for compounds **2**, **7**, **8** and **9**, and B(4) for compound **1**; the shortest is assigned to the PR_3 ligand that is *trans* to the S(7) vertex, whereas the intermediate Rh–P distances correspond to the phosphine groups that occupy positions *transoid* to the B(3)–B(4) edge of the cluster. This trend suggests that a boron vertex has a stronger *trans*-effect than either a B–B edge or a sulfur vertex in metallathiaboranes. Overall, there are no

significant differences in the corresponding distances and angles among the five {$RhSB_9H_9L$} clusters [where L = H (**1**), NC_5H_5 (**2**) or $PMePh_2$ (**9**)], although it may be noted that the Rh(8)–S(7) length in the hydridorhodathiaboranes **2** and **9** is *ca.* 0.05 Å longer than in the other derivatives, suggesting a higher structural *trans*-effect of the hydride ligand compared to the phosphines, PPh_3, $PMePh_2$, PMe_2Ph and PMe_3.

Bonding considerations

In view of the relevance of this set of compounds to the catalytic potential of the {$RhSB_9$} system,[2–4] the electronic constitution of the clusters, particularly with regard to the rhodium centre, merits consideration. The *bis*-(PR_3)-ligated rhodathiaboranes, **1**, **4**, **5** and **6**, could be regarded as formally 'unsaturated' clusters, with the "unsaturation" arising from the tendencies of rhodium to adopt a square-planar 16-electron metal configuration.[8,12,13]

Thus, these species could be described as Rh(I) complexes of $\{RhL_2\}^+$ with $\{nido\text{-}SB_9H_{10}\}^-$ fragments acting as bidentate ligands in a *tetrahapto* fashion, with the rhodium centre contributing two orbitals into the cluster bonding scheme. Bearing in mind the basic synthesis of **1** from $[RhCl(PPh_3)_3]$, it is reasonable to consider the {SBH_{10}} fragment in compound **1** as an LX ligand that formally replaces both the PPh_3 and the chlorine ligand in the Wilkinson's catalyst. Therefore, the attribution of the oxidation state +1 to the rhodium centre in these *bis*-(PR_3)-ligated clusters is reasonable. In accord with this, the ^{11}B NMR shielding pattern in compound **1** and its *bis*-(ligand) congeners **4**, **5** and **6** is clearly related to that of *nido*-6-SB_9H_{11} itself (Fig. 3, bottom two traces).[14] With three *exo*-polyhedral ligands on the metal centre, the situation in the *tris*-(PR_3)-ligated compounds **7** and **8** is potentially somewhat different. In principle, Wade's rules[15,16] would allocate to a {RhL_3} fragment a contribution of three orbitals and three electrons to the cluster framework. If this were the case, then the stereochemistry around the metal centre could be described as pseudo-octahedral, with three bonding vectors mainly directed towards the sulfur vertex, the boron atom B(9), and the B(3)–B(4) edge, and with the other three to the three *exo*-polyhedral ligands [Fig. 1 (b)]. Therefore, a description of **7** and **8** as Rh(III) octahedral complexes of $\{RhL_3\}^{3+}$ with a tridentate tetrahapto *arachno*-type $\{SB_9H_{10}\}^{3-}$ ligand, might at first sight be reasonable from the electron-counting rules approach as well as from a metal-to-ligand coordinative interaction. However, this would imply that the clusters of these *tris*-(ligand) species would have quite different electronic structures from the *bis*-(ligand) species, which would not be consistent with the similarities (a) of the cluster ^{11}B NMR shielding patterns (Fig. 3, centre trace) and (b) of the cluster dimensions among all the *bis*- and *tris*-ligated compounds **1**, **4**, **5**, **6**, **7** and **8**. These last two considerations suggest closely related electronic structures, and thence imply that **7** and **8** are best regarded as eighteen-electron rhodium(I) species, with five implied bonding vectors, two directed into the cluster as with compounds **1**, **4**, **5**, and **6**, with the other three directed towards the three phosphine ligands. This conclusion is supported by comparison of the ^{11}B nuclear shielding patterns with that of a cluster compound of the eleven-vertex {*nido*-8,7-MSB_9} configuration that does have a three-orbital cluster contribution from the metal centre, *e.g.* [8-(η^5-C_5Me_5)-*nido*-8,7-$IrSB_9H_{10}$] (**10**)[17] with an octahedral Ir(III) centre (Fig. 3, upper

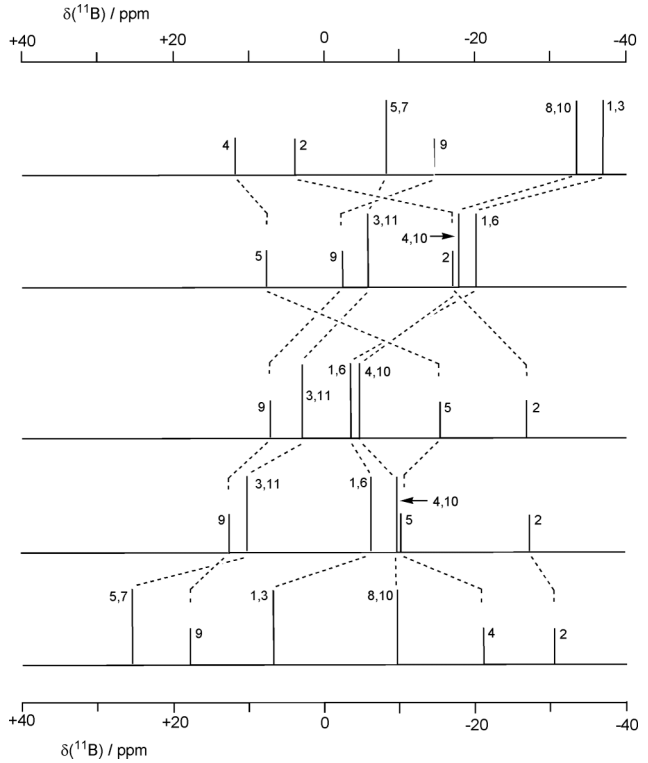

Fig. 3 Stick diagrams representing the chemical shifts and relative intensities in the ^{11}B NMR spectra of *nido*-6-SB_9H_{11} (lowest trace), the *bis*-(ligand) species [8,8-$(PPh_3)_2$-*nido*-8,7-$RhSB_9H_{10}$] **1** (low centre trace), the *tris*-(ligand) species [8,8,8-$(PMe_2Ph)_3$-*nido*-8,7-$RhSB_9H_{10}$] **7** (centre trace), [8-(η^5-C_5Me_5)-*nido*-8,7-$IrSB_9H_{10}$] **10** (upper centre trace), and the [*arachno*-6-SB_9H_{12}]$^-$ anion (uppermost trace). The values for **1**, **7** and **10** are averaged across the pseudo-mirror-plane of the {SB_9} fragment for purposes of comparison. Hatched lines connect equivalent positions. Note the inversion of cluster nuclear shielding characteristics between **7** and **10** (see text).

centre trace). It can be seen that, comparing compound **10** to compounds **1**, **4**, **5**, **6**, **7** and **8**, there is a fundamental change in the cluster electronic structure, as manifested in the cluster ^{11}B shielding characteristics: an essential inversion of the overall shielding pattern. This inversion is characteristic of *nido versus arachno* ten-vertex cluster species,[18] and it can be seen (Fig. 3, top trace) that the pattern of the cluster shielding of the {SB_9} unit of compound **10** clearly relates to that of the *arachno* [6-SB_9H_{12}]$^-$ anion, rather than that of *nido*-6-SB_9H_{11}.

The electronic structure within the cluster of the B-ligated hydridorhodathiaborane **9** is closely related to those of compounds **7** and **8**. Wade's rules[16] could be taken to describe the {$RhH(PMePh_2)_2$} fragment as a three-orbital two-electron contributor to the cluster bonding, which would leave the rhodium centre with a formal oxidation state of three. The stereochemistry [Fig. 2 (b)] could thence be viewed in terms of a quasi-octahedral Rh(III) complex of an *arachno*-type $\{SB_9H_9(PMePh_2)\}^{2-}$ fragment with a $\{RhH(PMePh_2)_2\}^{2+}$ centre. Alternatively, however, the {*nido*-$SB_9H_9(PMePh_2)$} fragment in **9** could be regarded as a 'charge-compensated' neutral ligand acting in a bidentate *tetrahapto* fashion, resulting in a Rh(I) species. In view of the arguments enunciated in the previous paragraph, we favour this

second interpretation. The ^{11}B nuclear magnetic shielding pattern is consistent with this.

Ligand-exchange processes and mechanistic considerations

In order to obtain some mechanistic insights about the substitutional chemistry of [8,8-$(PPh_3)_2$-*nido*-8,7-$RhSB_9H_{10}$] (**1**) with monodentate phosphines, the reactions (small scale) were studied at low temperatures by NMR spectroscopy. The reaction of two equivalents of PMe_3 with the rhodathiaborane **1** at 223 K immediately forms the *bis*-(ligand) monosubstituted derivative **6** and the *tris*-(PMe_3)-ligated cluster **8**. Reaction of **1** with PMe_2Ph similarly gives mixed-ligand *bis*-(phosphine) **5** and *tris*-(ligand) **7**. The relative temperature-dependent broadening of the signals in the ^{31}P-{^{1}H} NMR spectra of **5** and **6**, together with GIAO nuclear-shielding calculations (see supplementary material†), suggest that the substitution in **1** takes place selectively by the displacement of the PPh_3 ligand that is *trans* to the S(7) vertex (Scheme 1).

The formation of {RhL_3}-containing species indicates that the addition of a third phosphine (PMe_3 or PMe_2Ph) to the rhodium centre in the presumed [8,8-$(PR_3)_2$-*nido*-8,7-$RhSB_9H_{10}$] intermediates (where PR_3 is PMe_3 or PMe_2Ph) is faster than the substitution reaction of PPh_3 in **5** and **6**. The results suggest that the presence of more basic and less sterically demanding phosphine ligands on the rhodium centre, facilitates the substitution of the second PPh_3 ligand in **5** and **6**, and that the resulting supposed di-substituted intermediates react faster with free PR_3 than the mono-substituted compounds (Scheme 2).

Under the same conditions, the ^{31}P-{^{1}H} spectrum of the reaction mixture of **1** with one equivalent of $PMePh_2$ at 223 K shows (a) two sharp doublets of doublets at $\delta(^{31}P)$ +25.0 and +20.0 ppm, (b) two minor broad signals at $\delta(^{31}P)$ +21.0 and +5.0 ppm that correspond to compound **4**, (c) a singlet due to free PPh_3 and (d) traces of the starting material (see Fig. S4, supplementary material†). The ^{1}H–{^{11}B} NMR spectrum at the same temperature exhibits signals at $\delta(^1H)$ –1.66 and –1.95 ppm in a 1 : 0.3 relative intensity ratio. The latter minor component is assigned to the *bis*-($PMePh_2$)-substituted species **4**, whereas the major component is reasonably identified as the mono-substituted intermediate [8,8-($PMePh_2$)(PPh_3)-*nido*-8,7-$RhSB_9H_{10}$] (**11**) (Fig. S4†). Upon addition of a second equivalent of $PMePh_2$, there is a clear decrease in the intensity of the ^{31}P signals of **11**, together with a marked broadening of the signals corresponding to **4**. Interestingly, a new broad doublet at $\delta(^{31}P)$ *ca.* +20 ppm is formed, and the signal of free $PMePh_2$ at $\delta(^{31}P)$ *ca.* –20 ppm is also very broad, suggesting that there is chemical exchange between the free ligand and the rhodathiaborane clusters (Fig. S4†). The ^{1}H–{^{11}B} NMR spectrum confirms these observations, showing a decrease in the intensities of the BHB signals at $\delta(^1H)$ –1.66 and –1.95 ppm and the appearance of a new broad peak at $\delta(^1H)$ –3.42 ppm with the highest relative intensity (Fig. S5†).

As the temperature is increased further, the ^{31}P signals of **11** disappear and the spectrum shows a broad doublet at $\delta(^{31}P)$ *ca.* +21 ppm and a very broad signal at *ca.* +5 ppm, overall resembling the spectrum of compound **4**. In addition, the signal from free $PMePh_2$ is virtually lost on the base line. The corresponding ^{1}H–{^{11}B} NMR spectra show a significant broadening in the signals at $\delta(^1H)$ –2.00 and –3.00 ppm, and a final coalescence to give a single peak at –2.28 ppm. These observations suggest strongly that, at low temperatures, the monosubstituted {(PPh_3)($PMePh_2$)} intermediate **11** and the *bis*-($PMePh_2$)-substituted species **4** are in equilibrium with the free phosphines and a *tris*-(PR_3)-ligated cluster compound (Scheme 3). In this regard, as commented in

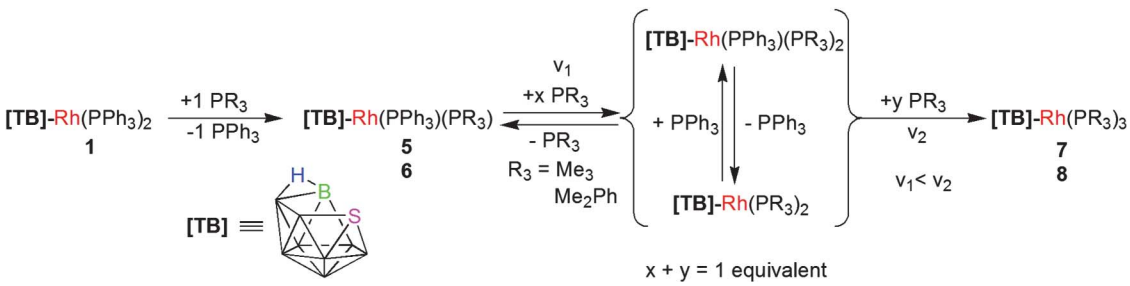

Scheme 2

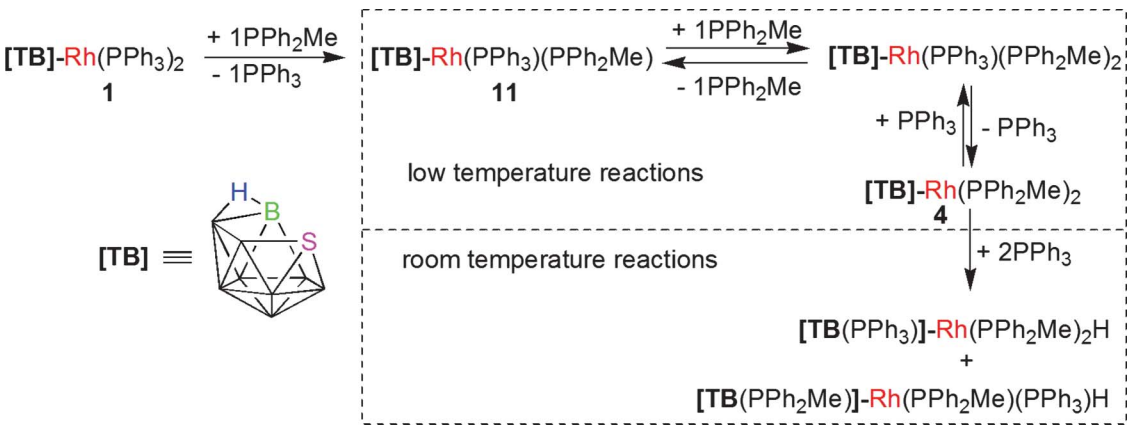

Scheme 3

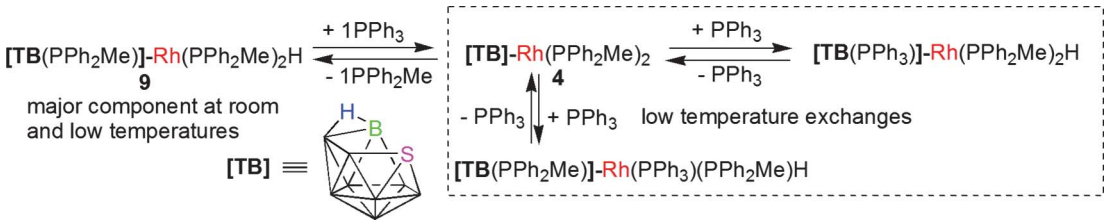

Scheme 4

the previous sections, a shift to higher field of around 2.00 ppm in the proton NMR signal of the BHB hydrogen atom in eleven-vertex *nido*-rhodathiaboranes is diagnostic of formation of the *tris*-(phosphine) $\{RhL_3\}$ species.

At room temperature, the equilibrium is completely shifted towards the disubstituted species **4**, but a lowering of the temperature back to 188 K reproduces the spectrum discussed above, demonstrating the reversibility of the system. However, at room temperature overnight, the system evolves to a mixture of two hydridorhodathiaboranes: one of them readily resembles **9** and the other is also very similar, but with small differences in the chemical shifts of the NMR spectra (Fig. S6†). This indicates that the presence of free PPh_3 in the media leads to formation of the mixed-phosphine species [8,8,8-$(PR_3)_2$(H)-*nido*-8,7-$RhSB_9H_9$-(PR_3)], in which the phosphine ligands can be combinations of PPh_3 and $PMePh_2$.

The temperature-dependent behaviour of B-ligated $[(PMePh_2)_2(H)RhSB_9H_9(PMePh_2)]$ **9** in the presence of one equivalent of PPh_3 was also studied. As the temperature decreases, the signals in the $^{31}P\{^1H\}$ NMR spectrum broaden significantly. At 223 K, this behaviour is accompanied with formation of small amounts of free $PMePh_2$ (Fig. S7†).

The corresponding $^1H–\{^{11}B\}$ spectrum shows concomitant broadening of the signals that arise from the BHB bridging hydrogen atom and the Rh–H hydride ligand. As the temperature is decreased further to 188 K, some of the signals sharpen in the $^{31}P\{^1H\}$ spectrum, and there is formation of new peaks; the $^1H–\{^{11}B\}$ NMR spectrum reflects these changes, showing now two BHB proton signals and three Rh–H hydride resonances with different relative intensity ratios (Fig. S8†). At room temperature, the NMR data show only the signals of compound **9**.

These observations are consistent with chemical exchange reactions involving free PPh_3 and the $PMePh_2$ ligands in the hydridorhodathiaborane **9** (Scheme 4). The observations described above permit a rudimentary reaction pathway to be described. In the conditions used for this work, the reaction rates of **1** with the more basic phosphines, $PMePh_2$, PMe_2Ph and PMe_3, to give the corresponding monosubstituted *bis*-(phosphine) derivatives, **4**, **5** and **6** by the displacement of the PPh_3 group *transoid* to the sulfur atom, appear to be similar. However the subsequent outcome of the reaction depends on the nature of the entering monodentate phosphine. Thus, the reaction rates of PMe_2Ph and PMe_3 with the supposed *bis*-substituted rhodathiaborane intermediates, [8,8-$(PR_3)_2$-*nido*-8,7-$RhSB_9H_{10}$], where $PR_3 = PMe_3$ or PMe_2Ph, are faster than with the monosubstituted precursors **5** and **6**, leading to the formation of the *tris*-(PR_3)-ligated species **7** and **8**. Since at low temperature we have not observed any stepwise formation of products that could indicate a rate-determining step, the rate of monosubstitution in **1** and the subsequent formation of the *tris*-(phosphine) $\{Rh(PR_3)_3\}$-containing species appear to be of the same order of magnitude. In contrast, the reaction rate of the monosubstituted *bis*-(ligand) $\{Rh(PPh_3)(PMePh_2)\}$ intermediate **11** with more $PMePh_2$ to give **4** is slower, and the NMR data suggest that a possible step for the substitution of the second PPh_3 phosphine in **11** is the formation of a *tris*-(ligand) rhodathiaborane species, *viz.* [$(PPh_3)(PMePh_2)_2$-*nido*-$RhSB_9H_{10}$], in equilibrium with compound **4** and free ligand (Scheme 3). This conclusion implies that the most plausible mechanism for the reactions of **1** with monodentate phosphines is associative, *i.e.* addition of phosphine to the *bis*-(phosphine) species **1**, followed by loss of phosphine to give the observed *bis*-(ligand) products. On the other hand, although the NMR data reveal an interesting chemical lability for **9**, it is not clear whether the formation of this hydridorhodathiaborane is also driven by the formation of a Rh-centred adduct that could promote the exchange of a Rh-bound $PMePh_2$ ligand with the terminal hydrogen atom at the boron B(9) position; or whether, alternatively, the B–$PMePh_2$ bond undergoes incipient dissociation, partially opening coordination sites on the cluster that could facilitate the exchange processes.

Conclusions

The series of compounds **4–9** illustrates nicely that the reactivity of the parent rhodathiaborane **1** with monodentate phosphines, and the composition and configuration of the resulting derivatives, are ultimately controlled by the nature of the phosphine. Thus the treatment of **1** with PPh_3 does not form *tris*-PPh_3-ligated species analogous to **7** and **8**, and the cluster remains formally unsaturated in the presence of triphenylphosphine.[1,6] In contrast, the less bulky and more basic phosphines, $PMePh_2$ and PMe_3, afford $\{Rh(L)_3\}$-vertices that confer one additional electron pair to the resulting eleven-vertex clusters compared with **1**. Interestingly, $PMePh_2$ exhibits an alternative behaviour: too bulky to form a stable $\{Rh(PMePh_2)_3\}$-fragment in this system, it has sufficient Lewis basicity to bind the boron B(9) vertex and to form a stable hydridorhodathiaborane. Variable-temperature experiments demonstrate the chemical lability of these eleven-vertex rhodathiaboranes, suggesting strongly that the most plausible mechanism for the substitution of the phosphine ligands is associative, implying the binding of a third phosphine at the rhodium centre. Likewise, the chemical lability exhibited by the hydridorhodathiaborane **9** could take place by associative processes at the $\{Rh(PMePh_2)_2(H)\}$ metal centre, which could be linked with an incipient partial dissociation of the B(9)-bound phosphine.

The treatment of **1** with monodentate phosphines is a convenient synthetic route for the alteration of the *exo*-polyhedral ligand sphere, confirming the tailorability of this eleven-vertex rhodathiborane system. Following the synthetic approach used for the preparation of **2**,[2] the *bis*-PR_3-ligated clusters, **4–6**, can (*a priori*) be easily modified by the treatment with pyridine, thus opening the door to the synthesis of hydridorhodathiaboranes that may exhibit an enhancement of the catalytic activity with respect to compound **2**. In the case of $PMePh_2$, the reaction with **1** affords directly a new hydridorhodathiborane with an interesting ligand non-rigidity, which augurs for a rich chemistry to complement and extend the reported reactivity of the pyridine-ligated rhodathiaborane **2** with unsaturated organic molecules.

Experimental

General procedures

Reactions were carried out under an argon atmosphere using standard Schlenk-line techniques. Solvents were obtained dried from a Solvent Purification System marketed by Innovative Technology Inc. The commercially available phosphines PMe_3, PMe_2Ph and $PMePh_2$ were used as received without further purification. The eleven-vertex rhodathiaborane [8,8-$(PPh_3)_2$-*nido*-8,7-$RhSB_9H_{10}$] (**1**) was prepared according to the literature method.[6] Preparative thin-layer chromatography (TLC) was carried out using 1 mm layers of silica gel G (Fluka, type GF254) made from water slurries on glass plates of dimensions 20 × 20 cm and dried in air at 25 °C. Infrared spectra were recorded on a Perkin-Elmer Spectrum 100 spectrometer, using a Universal ATR Sampling Accessory. NMR spectra were recorded on Bruker Avance 300-MHz AV, 400-MHz and 500 MHz spectrometers, using ^{31}P-{^1H}, [^{31}P–^1H]-HMBC, ^{11}B, ^{11}B–{^1H}, ^1H, ^1H–{^{11}B} and ^1H–{^{11}B(selective)} techniques. ^1H NMR chemical shifts were measured relative to residual proton resonances in the deuterated solvents used, and are reported in ppm relative to tetramethylsilane. ^{11}B chemical shifts are quoted relative to [$BF_3(OEt)_2$)] and ^{31}P chemical shifts are quoted relative to 85% aqueous H_3PO_4. Note that the values for $^1J(^{11}B–^1H)$ quoted are from the measured doublet maximum-to-maximum peak separation at room temperature in the solvents specified, and, for broader resonances in particular, will generally be smaller than the real coupling constant $^1J(^{11}B–^1H)$. Mass spectrometric data were recorded on a MICROFLEX instrument operating in either positive or negative modes, using matrix-assisted laser desorption/ionization (MALDI). A nitrogen laser of 337 nm (photon energy of 3.68 eV) was used for the ionization processes, and the molecules under study were protected with a matrix of *trans*-2-[3-(4-*tert*-butylphenyl)-2-methyl-2-propenylidene]malononitrile (DCTB).

Criteria for purity for the *bis*-(ligand) species **4**, **5** and **6**, which are straightforward analogues of the well-characterised species **1** were clean multinuclear NMR spectra allied with mass spectrometric confirmation of the molecular ions.

X-ray crystallography

X-ray diffraction data for compounds **8** and **9** were collected on the BM16 CRG beam line at the ESRF. We mounted single crystals of both complexes on micro Mount supports and were covered with perfluoropolyether. Data were measured in a single axis HUBER diffractometer, equipped with Oxford 600 Cryosystem open-flow nitrogen cryostat (100(1) K), using Silicon(111) monochromated synchrotron radiation ($\lambda = 0.73780$ Å). Intensities were integrated with HKL2000 suite[19] and corrected for absorption using a multiscan method applied with the SORTAV program.[20] The structures were solved and refined using the programs SHELXS-97[21] and SHELXL-97[22] respectively. Anisotropic displacement parameters were used in both refinements for all non-disordered atoms. In the case of **8**, a minor disorder (0.917 & 0.083(2) occupancy factors) affected the coordination of the sulfur atom to the metal. In the case of **9**, a clear situation of disorder involved a phenyl ring of one of the metal-bonded phosphines; this disorder was modelled on the base of two slightly displaced phenyl rings with similar occupancy factors (0.422 & 0.578(9)). Additionally, in the crystal structure of **9**, the presence of a highly disordered solvent molecule—interpreted as *n*-hexane—was also identified. The electronic density in the solvent region was estimated with PLATON/SQUEEZE program,[23,24] and eventually five residual peaks with complementary occupancies were included in the refinement to compensate for the presence of half a hexane molecule. For both structures, hydrogen atoms of the phosphine ligands were included in calculated positions and allowed to refine riding on their parent carbon atoms; the hydrogen atoms of the borane cluster in both structures, and the hydride ligand in **9**, were included from the difference Fourier maps and refined as free isotropic atoms.

Crystal data for **8**: $C_9H_{37}B_9P_3RhS$, M = 450.56, crystal size 0.105 × 0.056 × 0.049 mm^3, orthorhombic, P_{bca}, a = 16.3060(10), b = 15.5790(10), c = 17.4840(10) Å, V = 4441.5(5) Å^3, Z = 8, D_c = 1.407 g cm^{-3}, μ = 1.088 mm^{-1}, 74697 measured, 5464 independent reflections (5211 observed), 261 parameters, R_{int} = 0.058, R_1 = 0.0252, $wR(F^2)$ = 0.0693. Crystal data for **9**: $C_{39}H_{49}B_9P_3RhS$. $\frac{1}{2}$ C_6H_{14}, M = 886.04, crystal size 0.10 × 0.08 × 0.02 mm^3, triclinic, P-1, a = 11.4960(10), b = 12.6030(10), c = 17.1240(10) Å, α = 75.9350(10), β = 82.6070(10), γ = 65.0700(10)°, V = 2181.4(3) Å^3, Z = 2, D_c = 1.349 g cm^{-3}, μ = 0.577 mm^{-1}, 43398 measured, 11291 independent reflections (10602 observed), 576 parameters, R_{int} = 0.0412, $R1$ = 0.0402, $wR(F^2)$ = 0.1105. Full crystallographic details of both complexes have been deposited with the Cambridge Crystallographic Data Centre with CCDC reference numbers 814662 (**8**) & 814663 (**9**).

Calculations

All calculations were performed using the Gaussian 03 package.[25] Structures were initially optimized using standard methods with the STO-3G* basis-sets for C, B, P, S, and H with the LANL2DZ basis-set for the metal atom. The final optimizations, including frequency analyses to confirm the true minima, together with GIAO nuclear-shielding calculations, were performed using B3LYP methodology, with the 6-31G* and LANL2DZ basis-sets. The GIAO nuclear shielding calculations were performed on the final optimized geometries, and computed ^{11}B and ^{31}P shielding values were related to chemical shifts by comparison with the computed value for B_2H_6 and H_3PO_4, which were taken to be $\delta(^{11}B)$ +16.6 ppm relative to the $BF_3(OEt_2)$ = 0.0 ppm standard, and $\delta(^{31}P)$ = 0.0 ppm, respectively.

Synthesis of [8,8-(PMePh$_2$)$_2$-*nido*-8,7-RhSB$_9$H$_{10}$] (4)

Compound 4. A Schlenk tube equipped with a magnetic stirrer was charged with [(PPh$_3$)$_2$RhSB$_9$H$_{10}$] (**1**, 180 mg, 0.24 mmol). The rhodathiaborane was dissolved in CH_2Cl_2 (15 mL), and $PMePh_2$ (89 μL, 0.48 mmol) was added (with a syringe) to the tube. The resulting orange solution was stirred at room temperature under an atmosphere of argon for 16 h. The reaction mixture was concentrated to *ca.* 0.5 mL. Slow addition of hexane produced an orange solid that was separated by decantation, washed with hexane, and dried *in vacuum* (0.129 g, 84%). ^{11}B NMR (160 MHz; $CDCl_3$; 298 K): δ 10.6 (1B, br, BH), −1.8 (1B, br, BH), −9.1 (1B, d, BH), −27.6 (1B, br, BH); ^{1}H–{^{11}B} NMR (300 MHz; $CDCl_3$; 298 K): δ 7.89–6.86 (20 H, m, Ph), 2.15 (1H, br s, BH), 1.81 (1H, br s, BH), 1.78 (1H, br s, BH), −1.61 (1H, br s, BHB); ^{31}P-{^{1}H} NMR (161 MHz; $CDCl_3$; 202 K): δ 21.8 (dd, $^1J_{RhP}$ = 149 Hz, $PMePh_2$, $^2J_{PP}$ = 38 Hz), 5.8 (dd, $^1J_{RhP}$ = 137 Hz, $^2J_{PP}$ = 38 Hz, $PMePh_2$), at 296 K these two doublet of doublets coalesce; ^{1}H NMR (400 MHz; $CDCl_3$; 202 K): δ 2.27 (3H, s, $^2J_{PH}$ = 9.7 Hz, PPh_2Me), 1.38 (3H, s, $^2J_{PH}$ = 7 Hz, $PMePh_2$), at 279 K these two singlets coalesce; ^{1}H NMR (400 MHz; $CDCl_3$; 327 K): δ 1.81 (6H, s, $^2J_{PH}$ = 7.5 Hz, $PMePh_2$); $\Delta G^{\ddagger} = 52 \pm 3$ kJ mol^{-1}.

Synthesis of [8,8-(PPh$_3$)(L)-*nido*-8,7-RhSB$_9$H$_{10}$] [L = PMe$_2$Ph (5), PMe$_3$ (6)]

Compound 5. PMe_2Ph (16.6 mL, 0.124 mmol) was added to a red solution of **1** (0.0473 g, 0.062 mmol) in dichloromethane at room temperature. The reaction mixture was stirred for 1 h under an argon atmosphere, then reduced in volume and applied to a preparative TLC plate. The chromatogram was developed with a mixture of 4 : 1 CH_2Cl_2/hexane, leading to the isolation an orange component of R_F = 0.8 that was characterized as **5** (0.0201 g, 0.0313 mmol, 51%); and a yellow product of R_F = 0.5 that was identified as **7** (0.0093 g, 0.014 mmol, 23%, see below). Compound **5**: ^{1}H NMR (500 MHz; $CDCl_3$; 298 K): δ 8.10–6.92 (20 H, m, Ph), 1.94 (3H, d, $^2J_{PH}$ = 11 Hz, P(CH_3)$_2$Ph$_2$), 1.29 (1H, s, BH), 1.17 (3H, d, $^2J_{PH}$ = 10 Hz, P(CH_3)$_2$Ph$_2$). ^{31}P-{^{1}H} NMR (161 MHz; $CDCl_3$; 298 K): δ 23.8 (1P, dd, $^1J_{RhP}$ = 132 Hz, $^2J_{PP}$ = 45 Hz, PPh_3), 10.7 (1P, dd, $^1J_{RhP}$ = 150 Hz, P(CH$_3$)$_2$Ph$_2$). Cluster ^{11}B and ^{1}H NMR data are summarized in Table 1. *m*/*z* (MALDI$^+$) 380 ({M-(PPh$_3$+H)}$^+$ isotope envelope; $P_1C_8H_{21}Rh_1S_1B_9$ requires 380).

Compound 6. Following the same procedure as above, 0.037 mg (0.048 mmol) of **1** was treated with 36.8 μL (0.097 mmol), and the resulting reaction mixture was separated by TLC, using a 3 : 2 ratio of CH_2Cl_2/hexane, The chromatogram gave two bands: red, R_F = 0.5, and yellow R_F = 0.2. The red component was characterized as compound **6** (0.0173 g, 0.030 mmol, 62%) and the yellow product was identified as **8** (0.0106 g, 0.018 mmol, 38%). Compound **6**: ν_{max}(ATR)/cm^{-1} 2918 m, 2849 m, 2517 s (BH), 2159 s, 2030 s, 1996 s. ^{1}H NMR (500 MHz; $CDCl_3$; 298 K): δ 7.67–6.79 (15 H, m, Ph), 1.30 (9H, d, $^2J_{PH}$ = 10 Hz, P(CH_3)$_3$). ^{31}P-{^{1}H} NMR (161 MHz; $CDCl_3$; 223 K): δ 25.1 (1P, dd, $^1J_{RhP}$ = 141 Hz, $^2J_{PP}$ = 38 Hz, PPh_3), 5.1 (1P, dd, $^1J_{RhP}$ = 107 Hz, $^2J_{PP}$ = 38 Hz, P(CH$_3$)$_3$). Cluster ^{11}B and ^{1}H NMR data are summarized in Table 1. *m*/*z* (MALDI$^+$) 319 ({M-(PPh$_3$+H)}$^+$ isotope envelope; $P_1C_3H_{19}Rh_1S_1B_9$ requires 319).

Synthesis of [8,8,8-(L)$_3$-*nido*-8,7-RhSB$_9$H$_{10}$] [L = PMe$_2$Ph (7), PMe$_3$ (8)]

Compound 7. 58 mg of **1** (0.076 mmol) was dissolved in 15 mL of CH_2Cl_2 in a Schlenk tube. 3.37 mL (0.23 mmol) of PMe_2Ph was added to the orange solution of the rhodathiaborane, and the reaction mixture was stirred at room temperature under an atmosphere of argon for 4 h. The reaction mixture was concentrated to *ca.* 0.5 mL. Slow addition of hexane produced an orange solid that was separated by decantation, washed with hexane, and dried *in vacuum* to give 0.0479 g of **6** (96%). Elemental analysis: found: C, 42.5; H, 6.5; P, 14.2%. $C_{24}H_{43}B_9P_3Rh_1S_1$ requires C, 43.9; H, 6.6; P, 14.2%. ν_{max}(ATR)/cm^{-1} 3055 m, 2915 m, 2545w, 2345 m, 2117 w, 1992 w (BH), 1432 w, 1296 m, 1280 m, 1001 m, 933 w and 895 w. ^{1}H NMR (500 MHz; $CDCl_3$; 298 K): δ 7.93–6.84 (aromatic), 2.01 (9H, d, $^2J_{PH}$ = 3 Hz, P(CH_3)$_3$), 1.91 (9H, d, $^2J_{PH}$ = 3 Hz, P(CH_3)$_3$), 1.68 (9H, d, $^2J_{PH}$ = 5 Hz, P(CH_3)$_3$), 1.59 (9H, d, $^2J_{P,H}$ = 10 Hz, P(CH_3)$_3$), 1.56 (9H, d, $^2J_{PH}$ = 7 Hz, P(CH_3)$_3$), 1.33 (9H, d, $^2J_{PH}$ = 8 Hz, P(CH_3)$_3$). ^{31}P-{^{1}H} NMR (202 MHz; $CDCl_3$; 300 K): δ +11.6 (1P, dt, $^1J_{RhP}$ = 145 Hz, $^2J_{PP}$ = 27 Hz), −11.8 (1P, dt, $^1J_{RhP}$ = 145 Hz, $^2J_{PP}$ = 20 Hz), −24.2 (1P, d, br, $^1J_{Rh-P}$ = 81 Hz); cluster ^{11}B and ^{1}H NMR data are summarized in Table 3. *m*/*z* (MALDI) 381 {M–PMe$_2$Ph}$^+$ isotope envelope: $P_1C_8H_{21}Rh_1S_1B_9$ requires 381 and complete molecule $P_2C_{16}H_{32}Rh_1S_1B_9$ requires 519).

Compound 8. Following the same procedure as with **6** above, 141.3 mg (0.18 mmol) of **1** were treated with 42.0 mg (0.55 mmol) of PMe_3. Yield: 70.6 mg, 0.15 mmol, 82%. Elemental analysis: found: C, 22.9; H, 7.9; P, 19.6%. $C_9H_{37}B_9P_3Rh_1S_1$ requires C, 22.9; H, 7.9; P, 19.7%. IR(ATR): ν_{max}/cm^{-1} 3422 w, 2927 w, 2909 w, 2551 m, 2503 w, 2474 m (BH), 1645 s, 1433 m, 1418 w, 1303 m, 1282 w, 1261 m, 1093 m, 1038 m, 957 s, 910 w, 722 m. ^{31}P-{^{1}H} ($CDCl_3$; 223 K) and ^{1}H NMR ($CDCl_3$; 300 K) ordered as δ(^{31}P) (intensity, multiplicity, $^1J_{Rh-P}$, $^2J_{P-P}$) [δ(^{1}H) of directly bound CH_3 groups, $^2J_{P-H}$]: +3.2 (1P, dt, $^1J_{Rh-P}$ = 124 Hz, $^2J_{PP}$ = 25 Hz) [1.54, d, $^2J_{P-H}$ = 10 Hz], −25.3 (1P, ddd, $^1J_{RhP}$ = 127 Hz, $^2J_{PP}$ = 25 Hz, $^2J_{P-P}$ = 33 Hz) [1.59, d, $^2J_{PH}$ = 10 Hz], −30.6 (1P, broad d, $^1J_{Rh-P}$ = 87 Hz) [1.45, d, $^2J_{PH}$ = 7 Hz]; cluster ^{11}B and ^{1}H NMR data are summarized in Table 3. *m*/*z* (MALDI$^+$) 471 (M$^+$ isotope envelope; $P_3C_9H_{37}Rh_1S_1B_9$ requires 471).

Synthesis of [8,8,8-(PMePh$_2$)$_2$(H)-*nido*-8,7-RhSB$_9$H$_9$-9-(PMePh$_2$)] (9)

0.608 g (0.79 mmol) of **1** in 15 mL of CH_2Cl_2 were treated with 0.44 mL (2.38 mmol) of PPh_2Me in a Schlenk tube under argon at room temperature. After two hours of vigorous stirring, hexane was added and the resulting solid was separated by decantation, washed with hexane, and dried in vacuum to give 0.615 g (0.73 mmol; 93%) of **9**. Elemental analysis: found: C, 51.8; H, 5.54; P, 11.0%. $C_{39}H_{49}B_9P_3Rh_1S_1$ requires C, 55.6; H, 5.9; P, 11.0%. IR(ATR): ν_{max}/cm^{-1} 3054 w, 2921 w, 2852 w, 2519 m (BH), 2050 sh (RhH), 1585 s, 1572 s, 1481 m, 1433 w, 1093 m, 1026 m, 999 m, 881 w, 738 w, 690 w. ^{1}H–{^{11}B} NMR (500 MHz; $CDCl_3$; 298 K) δ 7.69–6.90 (aromatic); other NMR data are summarized in Table 3. *m*/*z* (MALDI$^+$) 641 ({M-2HPMePh$_2$}$^+$ isotope envelope. $P_2C_{26}H_{34}Rh_1S_1B_9$ requires 641).

Variable-temperature NMR studies

The reactions of **1** with $PMePh_2$ and PMe_3 were studied at low temperature by NMR spectroscopy. 15 mg of the rhodathiaborane was put in a 5 mm NMR tube, and dissolved in 0.6 mL of CD_2Cl_2 under an argon atmosphere. To the resulting orange solution, 1 equivalent of the phosphine was added at the temperature of liquid nitrogen. The tube was transported immersed in liquid nitrogen and it was inserted into an NMR probe head with the temperature set to 188 K. The ^{1}H–$\{^{11}B\}$ and ^{31}P-$\{^{1}H\}$ NMR spectra was then measured; the sample was then heated to 223 K and the ^{1}H and ^{31}P-$\{^{1}H\}$ spectra measured at this temperature. The sample tube was removed from the NMR instrument and transported (immersed in liquid nitrogen) to the Schlenk line, where a second equivalent of phosphine was added at low temperature. The resulting reaction mixture was studied at different temperatures (see supplementary material: Fig. S4–S6†).

Following the same procedure, 15 mg of the hydridorhodathiaborane **9** was dissolved in 0.6 mL of CD_2Cl_2 with 1 equivalent of free PPh_3, and the resulting yellow solution was studied over a range of temperatures by ^{1}H–$\{^{11}B\}$ and ^{31}P-$\{^{1}H\}$ NMR spectroscopy (Fig. S7–S8†).

Acknowledgements

We acknowledge the Spanish Ministry of Science and Innovation (CTQ2009-10132, CONSOLIDER INGENIO, CSD2009-00050, MULTICAT and CSD2006-0015, Crystallization Factory) for support of this work. B.C. thanks the 'Diputación General de Aragón' for a pre-doctoral scholarship. M.K. thanks the Universities of Würzburg (Germany) and Zaragoza (Spain) for support through the Erasmus Exchange Program. We also thank BM16 staff, specially to A. Labrador, for their valuable assistance during X-ray diffraction measurements.

Notes and references

1 G. Ferguson, M. C. Jennings, A. J. Lough, S. Coughlan, T. R. Spalding, J. D. Kennedy, X. L. R. Fontaine and B. Stibr, *J. Chem. Soc., Chem. Commun.*, 1990, 891.
2 A. Álvarez, R. Macías, M. J. Fabra, F. J. Lahoz and L. A. Oro, *J. Am. Chem. Soc.*, 2008, **130**, 2148.
3 A. Álvarez, R. Macías, J. Bould, M. a. J. Fabra, F. J. Lahoz and L. A. Oro, *J. Am. Chem. Soc.*, 2008, **130**, 11455.
4 A. Álvarez, R. Macías, J. Bould, C. Cunchillos, F. J. Lahoz and L. A. Oro, *Chem.–Eur. J.*, 2009, **15**, 5428.
5 R. Macías, N. P. Rath and L. Barton, *Organometallics*, 1999, **18**, 3637.
6 S. Coughlan, T. R. Spalding, G. Ferguson, J. F. Gallagher, A. J. Lough, X. L. R. Fontaine, J. D. Kennedy and B. Štíbr, *J. Chem. Soc., Dalton Trans.*, 1992, 2865.
7 A. Álvarez, R. Macías, M. J. Fabra, M. L. Martin, F. J. Lahoz and L. A. Oro, *Inorg. Chem.*, 2007, **46**, 6811.
8 R. Macías, J. Bould, J. Holub, J. D. Kennedy, B. Štíbr and M. Thornton-Pett, *Dalton Transactions*, 2007, 2885.
9 B. Štíbr, T. Jelínek, J. D. Kennedy, X. L. R. Fontaine and M. Thornton-Pett, *J. Chem. Soc., Dalton Trans.*, 1993, 1261.
10 G. Ferguson, A. L. Lough, S. Coughlan and T. R. Spalding, *Acta Crystallogr., Sect. C: Cryst. Struct. Commun.*, 1992, **48**, 440.
11 H. Beall, C. H. Bushweller, W. J. Dewkett and M. Grace, *J. Am. Chem. Soc.*, 1970, **92**, 3484.
12 J. D. Kennedy, in *The Borane-Carborane-Carbocation Continuum*, ed. J. Casanova, Wiley, New York, 1998, ch. 3, pp. 85–116.
13 M. P. Murphy, T. R. Spalding, C. Cowey, J. D. Kennedy, M. Thornton-Pett and J. Holub, *J. Organomet. Chem.*, 1998, **550**, 151.
14 M. Bown, X. L. R. Fontaine and J. D. Kennedy, *J. Chem. Soc., Dalton Trans.*, 1988, 1467.
15 K. Wade, *Adv. Inorg. Chem.*, 1976, **18**, 1.
16 K. Wade, *J. Chem. Soc., Chem Commun.*, 1971, 792.
17 K. Nestor, X. L. R. Fontaine, N. N. Greenwood, J. D. Kennedy and M. Thornton-Pett, *J. Chem. Soc., Dalton Trans.*, 1991, 2657.
18 M. Bown, X. L. R. Fontaine and J. D. Kennedy, *J. Chem. Soc., Dalton Trans.*, 1988, 1467.
19 Z. Otwinowski and W. Minor, in *Methods in Enzymology*, ed. J. R. M. S. C. W. Carter, Academic Press, New York, 1997, vol. 276, pp. 307–326.
20 R. H. Blessing, *Acta Crystallogr., Sect. A: Found. Crystallogr.*, 1995, **51**, 33.
21 G. M. Sheldrick, *SHELXS-97,* University of Göttingen, Göttingen, Germany, 1997.
22 G. M. Sheldrick, *Acta Crystallogr., Sect. A: Found. Crystallogr.*, 2008, **64**, 112.
23 A. L. Spek, *J. Appl. Crystallogr.*, 2003, **36**, 7.
24 P. v. d. Sluis and A. L. Spek, *Acta Crystallogr., Sect. A: Found. Crystallogr.*, 1990, **46**, 194.
25 M. J. Frisch, G. W. Trucks, H. B. Schlegel, G. E. Scuseria, M. A. Robb, J. R. Cheeseman, J. A. M. Jr., T. Vreven, K. N. Kudin, J. C. Burant, J.M. Millam, S. S. Iyengar, J. Tomasi, V. Barone, B. Mennucci, M. Cossi, G. Scalmani, N. Rega, G. A. Petersson, H. Nakatsuji, M. Hada, M. Ehara, K. Toyota, R. Fukuda, J. Hasegawa, M. Ishida, T. Nakajima, Y. Honda, O. Kitao, H. Nakai, M. Klene, X. Li, J. E. Knox, H. P. Hratchian, J. B. Cross, V. Bakken, C. Adamo, J. Jaramillo, R. Gomperts, R. E. Stratmann, O. Yazyev, A. J. Austin, R. Cammi, C. Pomelli, J. Ochterski, P. Y. Ayala, K. Morokuma, G. A. Voth, P. Salvador, J. J. Dannenberg, V. G. Zakrzewski, S. Dapprich, A. D. Daniels, M. C. Strain, O. Farkas, D. K. Malick, A. D. Rabuck, K. Raghavachari, J. B. Foresman, J. V. Ortiz, Q. Cui, A. G. Baboul, S. Clifford, J. Cioslowski, B. B. Stefanov, G. Liu, A. Liashenko, P. Piskorz, I. Komaromi, R. L. Martin, D. J. Fox, T. Keith, M. A. Al-Laham, C. Y. Peng, A. Nanayakkara, M. Challacombe, P. M. W. Gill, B. G. Johnson, W. Chen, M. W. Wong, C. Gonzalez and J. A. Pople, in '*GAUSSIAN 03 (Rev. C.02)*', Wallingford, CT, 2004.

